

Design of a vacuum-compatible high-precision monochromatic beam-position monitor for use with synchrotron radiation from 5 to 25 keV

R. W. Alkire,^{a*} G. Rosenbaum^a and G. Evans^b

^aBiosciences Division, Argonne National Laboratory, 9700 South Cass Avenue, Bldg 202, Argonne, IL 60439, USA, and ^bMRC Laboratory of Molecular Biology, Hills Road, Cambridge CB2 2QH, UK. E-mail: alkire@anl.gov

(Received 18 August 1999; accepted 3 December 1999)

The Structural Biology Center beamline, 19ID, has been designed to take full advantage of the highly intense undulator radiation and very low source emittance available at the Advanced Photon Source. In order to keep the X-ray beam focused onto the pre-sample slits, a novel position-sensitive PIN diode array has been developed. The array consists of four PIN diodes positioned upstream of a 0.5 μm -thick metal foil placed in the X-ray beam. Using conventional difference-over-the-sum techniques, two-dimensional position information is obtained from the metal foil fluorescence. Because the full X-ray beam passes through the metal foil, the true beam center-of-mass is measured. The device is compact, inexpensive to construct, operates in a vacuum and has a working range of 8 mm \times 10 mm that can be expanded with design modifications. Measured position sensitivity is 1–2 μm . Although optimized for use in the 5–25 keV energy range, the upper limit can be extended by changing metals or adjusting foil thickness.

Keywords: beam-position monitors; X-rays; detectors.

1. Introduction

Since the early days of synchrotron radiation, users have been concerned with position and stability of the X-ray beam. Changes in magnet cooling water temperature, power supply instabilities and vibrations from sources outside the facility have caused many problems for facility and beamline operators to overcome. Third-generation synchrotron sources with undulators pose even greater demands on positioning devices, given the increased heat load and distances of up to 55 m between the undulator and first optical element. It is no wonder that considerable effort has been devoted to developing 'white beam' position monitors (Mortazavi *et al.*, 1986; Johnson & Overluizen, 1989; Warwick *et al.*, 1992; Fauchet *et al.*, 1992; Sakae *et al.*, 1997; Hahn *et al.*, 1998; Shu *et al.*, 1998). Combined with advances in global orbit feedback technology, these devices have been able to limit displacement of the electron orbit to within a few micrometers, with the possibility of direct feedback detection in the sub-micrometer range (Miyahara & Mitsuhashi, 1992).

19ID focusing optics are able to produce uncollimated beam dimensions at the sample of 38 μm (vertical) \times 83 μm (horizontal) full width at half-maximum (FWHM). The photon flux density has been measured to be 3×10^{15} photons s^{-1} mm^{-2} at 12 keV and 100 mA. The high flux density and low convergence of the focused beam

permit further reductions in beam size through collimation, while retaining sufficient flux for fast data collection. These characteristics are extremely useful for investigating small samples. However, with collimating slit dimensions of 50 μm \times 50 μm or less, it is necessary to have precise monochromatic beam positioning.

For wide (5–10 mm) beam dimensions, a vibrating reed has been used to optimize sample positioning (Khalid *et al.*, 1990). When the beam size reaches 1–2 mm a quadrant PIN photodiode can be used to intercept the edges of the focused beam while passing the main beam undisturbed (*e.g.* Models AXUV-PS1 or AXUV-PS2; International Radiation Detectors, California, USA). Current density limits of the photodiodes prevent detection of the full undulator beam, limiting the working range of these devices to a few millimeters. In addition, the outer edges of the X-ray beam may not accurately describe the center-of-mass of the focused beam, leading to errors in positioning.

For narrow-beam applications the method of choice has been the split ion chamber (Koyama *et al.*, 1989; Schildkamp & Pradervand, 1995). The split ion chamber is essentially 'non-interfering', is capable of less than 5 μm positioning accuracy (Billing, 1988), and has a linear working range of a few millimeters. Split ion chambers can, however, suffer from recombination and space charge effects and report false readings when operated near a strong scattering source if care is not used in their design

and operation (Schildkamp & Pradervand, 1995). In addition, the device is not vacuum compatible and must be relatively long, typically ≥ 5 cm in length, to achieve adequate signal strength. Since split ion chambers measure in only one dimension, two such devices are required to obtain horizontal and vertical information simultaneously.

An alternative to the split ion chamber has been developed for small beams using a thin CVD diamond photo-detector (Bergonzo *et al.*, 1999). This device has been optimized for low-energy X-rays *e.g.* 2–10 keV, and demonstrates relatively high position sensitivity. However, position resolution of the device is currently beam-size dependent, with the best resolution obtained for beam sizes close to half the inter-electrode spacing of 0.5 mm. Errors in determining the beam centroid may also occur since only the outer portion of the beam is used for position determination.

In this report we describe the design of a new monochromatic beam-position monitor using PIN photodiode detectors and fluorescence radiation generated from a metal foil in the path of the X-ray beam. The device is vacuum compatible, is only 2.0 cm long and can operate over a wide energy range. The primary purpose of the beam-position monitor will be to correct tune losses when changing the energy of the monochromator and to measure variations in beam position during data collection. Using calibration information, the amount and direction of adjustment necessary to keep the beam centered on the exit slits can be computed, thereby stabilizing and maximizing the X-ray intensity on the sample.

2. Detector design

PIN photodiodes have been used in a wide range of applications including EXAFS (Bouldin *et al.*, 1987), small-

angle scattering (Jemian & Long, 1990), reflectivity measurements (Storb *et al.*, 1991) and as a beam-position monitor in an ultrahigh vacuum environment (Southworth & Cowan, 1992). More recently, the idea of using thin metal foils as a source of fluorescent radiation for an incident-beam intensity monitor (Alkire & Rotella, 1997; Gauthier *et al.*, 1995) provided the basis for the present detector design. PIN photodiodes, when operated in photovoltaic mode, can be treated much like an ion chamber, except they have higher quantum efficiency and, therefore, higher signal-to-noise ratio. Fig. 1 illustrates the design of the photodiode array along with the position of the fluorescing metal foil and surrounding end-station components.

The array consists of four PIN diodes (Model S100V; UDT Sensors Inc., California, USA), positioned 90° apart on a plastic holder. Each diode measures $10 \text{ mm} \times 10 \text{ mm}$, with a small inactive area extending outside the 100 mm^2 region. The distance between the upper and lower diodes is 10.7 mm, while the horizontal diodes are spaced 12.6 mm apart. An $8.0 \text{ mm (V)} \times 10.6 \text{ mm (H)}$ opening has been machined into the plastic holder to provide a large unobstructed pathway for the X-ray beam. Downstream of the diode holder is the fluorescence source, typically an 11 mm-diameter $0.5 \mu\text{m}$ -thick foil of Cr ($K_{\text{edge}} 5989 \text{ eV}$, $K_{\alpha 1} 5415 \text{ eV}$) or Ti ($K_{\text{edge}} 4966 \text{ eV}$, $K_{\alpha 1} 4511 \text{ eV}$) (Henke *et al.*, 1993; Cauchois & Senemaud, 1978). Metal foils of this size are available commercially (ACF Metals Co. Inc., Arizona, USA) and can be acquired directly attached to a stainless steel washer without any additional substrate beneath the metal foil surface. Alternately, the metal foil can be deposited onto a thin Kapton film for additional support. Only non-substrate metal foils were used in this study. The foil is fixed in position with respect to the diodes, so that vertical or horizontal movement of the array does not change the foil position relative to the diodes.

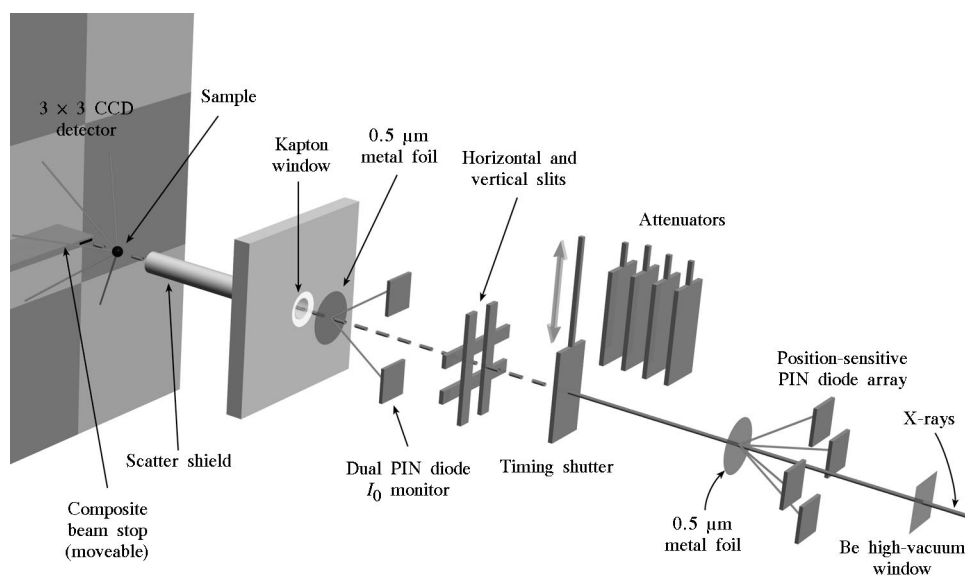


Figure 1

Diagram of the beam-position monitor and surrounding end-station components. The beam-position monitor consists of four $1 \text{ cm} \times 1 \text{ cm}$ PIN photodiodes located upstream of a $0.5 \mu\text{m}$ metal foil.

The stainless steel washer has an 11 mm internal diameter and the metal foil completely covers this opening. The washer is loaded into a high-purity aluminium shell, securing the metal foil in place and blocking any fluorescence that might be emitted by the stainless steel. The position of the metal foil is approximately 9 mm from the plane of the diodes. The outer diameter of the assembly is 44 mm, with a total thickness of 20 mm. The average cost of the device is a few hundred dollars, plus electronics.

After installing the metal foil, the completed assembly is inserted into the light-tight flight path, positioning the array at ~ 5.9 m downstream from the monochromator. The flight path, which also includes the timing shutter, filters and slit assembly, is evacuated to a rough vacuum. Diodes are unbiased and photocurrent signals are fed *via* an electrometer amplifier plus voltage-to-frequency converter to a scaler. Two motorized translation stages external to the vacuum (not shown) support the diode array assembly, allowing scanning in both vertical and horizontal directions for calibration and centering to the nominal beam position. Translation stages are driven by DC motors and position is measured using high-resolution optical linear encoders.

Care must be taken when transporting the metal foils and when evacuating or re-pressurizing the assembly, since modest differential pressure can break the foil when not mounted to a substrate. These conditions are not excessively restrictive, however, and the assembly has been cycled several times without damage to the foils.

The efficiency of a PIN diode depends upon the absorption cross section for silicon [$\mu(E)$] and the thickness of the active region of the diode. Since diode characteristics are fixed at the time of purchase, tuning the device to meet differing needs rests on the choice of metal foil.

Three primary criteria must be considered when selecting the foil. First, fluorescence yield, *i.e.* the amount of fluorescent radiation emitted per unit incident absorbed intensity, increases with atomic number. Second, the fluorescent energy should occur in a region where the spectral sensitivity of the PIN diode is relatively high. Third, it is advantageous to select an element that has no absorption edge in the operating energy range.

The first two criteria work in opposite directions. For *K*-edges the increase in fluorescence yield at high *Z* is offset by the decrease in diode sensitivity at higher emission energies. Fluorescence from *L*-edges at high *Z*, although advantageous with respect to diode sensitivity, is produced with lower yields (Vaughn, 1986) than *K*-edge fluorescence at low *Z*. Consequently, it is advantageous to use the *K*-edge of a low-*Z* element. The element should be chosen so that its *K*-edge falls below the desired operating energy range, thereby avoiding edge jumps that would require changing foils.

Optimal spectral sensitivity of the PIN diodes used in the array is the visible to ultraviolet range. However, X-ray sensitivity is still high enough to provide adequate signal strength using fluorescence emissions from 4 to 8 keV. Because $\mu(E)$ for silicon decreases with increasing energy,

it is advantageous to keep the fluorescent X-ray energy relatively low.

In addition to the first three criteria, the material must also be chemically stable, tolerate high doses of radiation, and be easily manufactured into thin foils of uniform thickness without voids, *e.g.* 0.5–2 μm . Ti, Cr, Fe, Co, Ni, Cu and Zn meet these requirements and are commercially available at low cost. Their *K*-edges are near the typical crystallographic envelope, *e.g.* 5–25 keV, and their emission energies are low, ranging between 4.5 and 8.6 keV.

PIN diodes have been shown to maintain linear response over seven orders of magnitude, up to a maximum photocurrent of 0.1–1 mA (Jemian & Long, 1990). At 191D we have observed non-linear photocurrent output generated by a commercial diode when exposed directly to the monochromatic beam due to the high brilliance of the undulator radiation. Using a lower flux density signal derived from the primary beam is, therefore, a key factor in maintaining optimal performance of the detector array.

PIN diodes are light sensitive, so care must be taken to minimize stray light when placing the diode array near Kapton or aluminized Mylar vacuum windows. To minimize detection of background fluorescence and/or scattered radiation emitted from the Be window assembly, the upstream side of the plastic holder has been masked with lead tape.

3. Results and discussion

Calibration of the diode array response *versus* beam position is acquired in reverse mode: the array, mounted on a translation stage, is scanned relative to a stationary beam. Vertical calibration, for example, is computed by subtracting the bottom diode signal from the top diode signal, then dividing by their sum. This method is widely referred to as the difference-over-the-sum (difference/sum) technique. With independent readouts, both directions can be monitored simultaneously. Since the difference/sum is a normalized signal, it is inherently independent of beam

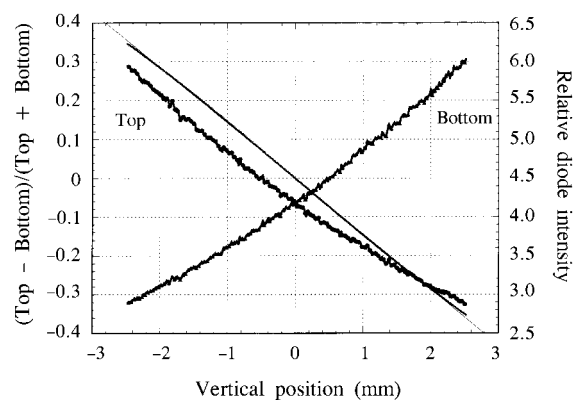


Figure 2

Vertical calibration at 8 keV in air using Cr metal. A straight line has been laid over the difference/sum curve to illustrate the degree of linearity.

intensity and photon energy. In addition, because the entire beam is used in the measurement, the true center-of-mass is measured.

In the following discussion and in Figs. 3–5, deviations of the measured response from a linear or polynomial fit to the measured data are expressed in position rather than in difference/sum units. This illustrates better the significance of the deviations for beam-position monitoring. Linear fits of the slope are used for conversion.

Fig. 2 illustrates the top and bottom diode signals acquired during a vertical calibration scan using a Cr foil at 8 keV. To ensure the highest possible accuracy for this measurement, *i.e.* to avoid strain on the translation stage induced by atmospheric pressure on the vacuum bellows, this measurement was performed in air. Also plotted are the difference/sum ratios along with a linear fit overlay showing a high degree of linearity over the 5 mm range. The slope is negative because the array is translated relative to the beam.

Deviations from linearity for the 5 mm vertical calibration in Fig. 2 are presented in Fig. 3 (solid line). Expressed in position, deviations are within $\pm 25 \mu\text{m}$ except for the outermost 0.25 mm. It is obvious from Fig. 3 that the deviations are far above random noise. Indeed, Fig. 3 (dashed line) shows the result of a calculation[†] of the difference/sum of the solid angles of fluorescence accepted by the diode pair as the source of the fluorescence moves relative to the diode array. Assumptions for this calculation were uniform response of the diodes and an isotropic fluorescence field. Air absorption, air scatter and corrections to diode sensitivity *versus* angle of incidence have been neglected. Both curves are closely matched in shape and are symmetric about the center of the scan range. This demonstrates that the smoothly varying features of the measured difference/sum curve are systematic. In practical terms a third-order polynomial is sufficient to fit the 5 mm vertical calibration scan with a standard deviation of $0.98 \mu\text{m}$. This is about the limit of calibrated response. The limit of detection of beam motion as evidenced by the high degree of reproducibility between scans is well below $1 \mu\text{m}$.

While it is useful to maintain position linearity over several millimeters, primary use of this device will be concentrated in a much smaller range. At 19ID, systematic and random beam motion are commonly well below 1 mm . This allows calibrations to be performed over a smaller range and thus permits the use of a linear fit instead of a polynomial. Table 1 lists the r.m.s. residuals arising from

[†] We define $z = 0$ as the plane of the diodes and $xs = (xs, ys, zs)$ as the source of the fluorescence radiation. The solid angle subtended by a diode element $dx dy$ at point $x = (x, y, 0)$ is $d\Omega = dx dy zs / |x - xs|^{-3/2}$. Double integration yields $\Omega = \arctan[x(x^2 + y^2 + zs^2)^{-1/2}/zs]$. The integration ranges are $-w/2 \leq x \leq +w/2$ and $y_1 \leq y \leq y_1 + h$, where w = width of diode, y_1 = center of opening for beam to edge of diode, and h = height of diode. *Mathematica 2.2* and *3.0* (Wolfram Research Inc., IL, USA) has been used for algebraic and numerical integrations. For calculations of the effect of the beam size on the difference/sum the point source at xs has been replaced by a Gaussian source distribution centered at xs with widths $\sigma = 0, \dots, 2.5 \text{ mm}$ ($0, \dots, 6 \text{ mm FWHM}$).

Table 1

Deviation (r.m.s.) from linear fit for 1 mm in-vacuum calibration scans.

	8 keV		12 keV	
	Cr	Ti	Cr	Ti
Vertical (μm)	3.3	2.4	2.8	3.3
Horizontal (μm)	0.7	1.1	1.1	1.1

linear fits to vertical and horizontal calibration scans over a 1 mm range using Cr and Ti metal foils at 8 keV and 12 keV performed under vacuum. Calculations assuming different beam sizes show that the difference/sum ratio for a 1 mm calibration varies by less than 1% for beam sizes up to 6 mm in either direction.

The vertical calibrations have two to four times larger residuals than the horizontal scans. The suspicion that this was caused by structure in the foil was investigated by rotating the foil by 90° and using the same part of the foil for both scans. After rotation, deviations from linearity were again a factor of two greater for the vertical direction compared with the horizontal direction. However, multiple scans in either direction and in either foil orientation were reproducible to better than $\pm 1 \mu\text{m}$ and indicate that noise in the diode signal is not responsible for the difference. It appears that the differences between vertical and horizontal directions are systematic. However, model calculations show that the difference in diode separation, which should rather favor the vertical diode pair, does not have a large effect on the difference/sum values. This points to differences in the accuracy of the translation of the array.

After repeated examination of several metal foils it became apparent that non-uniform flatness of the foil also produced deviations from linearity. Uniformly flat foils can be acquired attached to washers, but a flatness specification was not requested when purchasing the foils for this study.

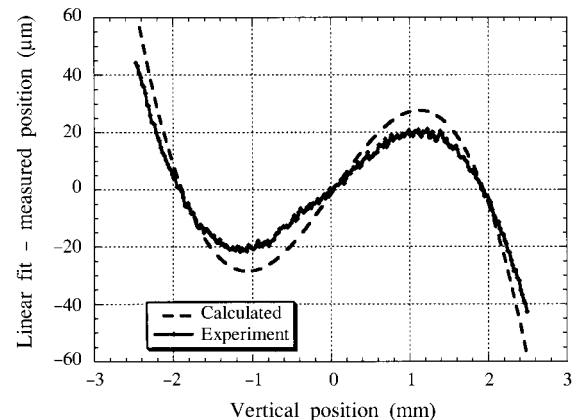


Figure 3

A linear fit to the vertical difference/sum curve was used to predict motor positions. Differences between the linear fit (predicted) and measured values are shown above. A theoretical calculation (dashed curve) has the same basic shape and symmetry as the experimental curve, indicating that the differences are systematic and can be included in the calibration.

Table 2

In-vacuum calibration constants calculated as the slope of linear fits to difference/sum data *versus* translation stage position and against monochromator tune and roll angles.

Translation calibrations were performed over the central 1 mm range. The central (FWHM) region of the tune curve and a roll range of 0.50 mrad were used for angular calibrations. The numbers shown in parentheses are the standard deviations of the last digit of the value listed, computed from multiple measurements. The last column ('Calculated') shows the calibration constants derived from the calculated solid angles of fluorescence radiation intercepted by the diodes as a function of beam position.

	8 keV		12 keV		Calculated
	Cr	Ti	Cr	Ti	
Vertical (mm^{-1})	0.162 (1)	0.167 (1)	0.161 (1)	0.190 (1)	0.1582
Horizontal (mm^{-1})	0.1641 (1)	0.1703 (1)	0.1676 (3)	0.2067 (5)	0.1586
Tune (vertical) (mrad^{-1})	1.54 (2)	1.82 (2)	1.37 (1)	1.53 (1)	
Roll (horizontal) (mrad^{-1})	-0.411 (8)	-0.459 (5)	-0.327 (1)	-0.368 (1)	

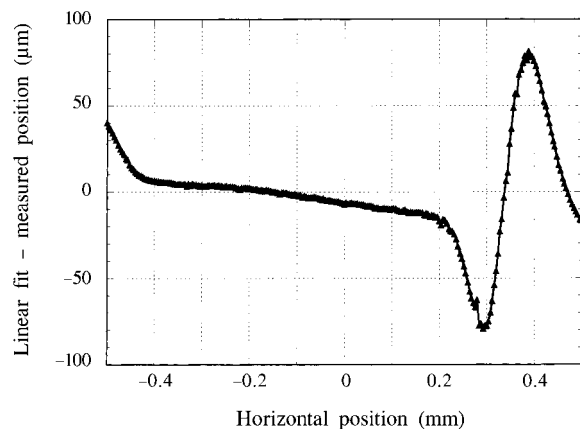
Most of the Cr foils had a relatively smooth appearance, but some Ti foils displayed noticeable structure. Fig. 4 shows the deviations from linearity for a horizontal calibration using a wrinkled Ti foil under vacuum. The flat region of the scan has an estimated r.m.s. deviation of 6 μm but increases to $\pm 80 \mu\text{m}$ peak at one end of the scan range.

Table 2 shows calibration constants for scans using both Cr and Ti foils at 8 keV and 12 keV. Two different kinds of scans were performed with the assembly mounted inside a vacuum enclosure: first, moving the array relative to the stationary beam using vertical and horizontal translation stages and, second, with the array position fixed using the monochromator tune and roll motion to generate vertical and horizontal changes in beam position at the foil. Table 2 shows that in-vacuum slope calibrations *versus* beam position for Cr and Ti are equivalent within $\sim 10\%$. This is to be expected since the difference/sum ratio should only depend upon the geometry of the array if the diode signal is generated by fluorescent radiation alone. The same should be true for the energy dependence and, indeed, calibrations for Cr varied little as a function of energy. However, Ti exhibited significant energy dependence. This suggests that a fraction of the diode signals is generated by scatter of the incident beam off the foil. The angular distribution of scattered radiation and, thus, its contribution to the diode signal, changes with energy. The difference between Cr and Ti is attributable to the higher fluorescence energy and yield of Cr, which makes the contribution of scattered radiation to diode current relatively smaller. However, calibrations are always reproducible, making it possible to determine precise calibration information at any energy.

Photocurrent output (in vacuum) from the vertical diodes using Cr was 2.7 μA at 8 keV and 0.42 μA at 12 keV, normalized to 100 mA X-ray ring current. For Ti, photocurrents were 0.88 μA and 0.14 μA at 8 keV and 12 keV, respectively. All levels are within the linear detection range of the PIN diodes and accurately measurable with any commercial electrometer amplifier. At 19 keV, photocurrent from Ti metal was 0.2 μA in the vertical direction (note: third-order undulator emission at 19 keV is higher than first-order emission at 12 keV). These sustained high photocurrent levels make the fluorescent technique useful over a wide energy range and provide several orders of

magnitude more signal than techniques based on scattered radiation alone (Silfhout, 1999).

Another contribution to the diode signal could potentially arise from thermal radiation from the foil. The monochromatic beam deposits 0.73 mW at 12 keV and 3.9 mW at 8 keV in the Cr foil, and 0.37 mW and 2.0 mW, respectively, in the Ti foil, assuming 100 mA storage ring current and first-order undulator radiation. The temperature rise in the center of the foil is approximately 2 K at 12 keV, 11 K at 8 keV for Cr, and 6 K and 30 K for Ti, respectively. Although less power is deposited in the Ti foil, the estimated temperature rise is greater because Ti has one-quarter the thermal conductivity of Cr. While the temperature rises are small and the radiative heat dissipation is a small fraction of the conductive pathway (1–2% for Cr, 5–10% for Ti), the ratio of the total power of thermal emission over fluorescence emission is 0.05–0.08 for Cr and 0.3–0.5 for Ti. However, the photon energy at the peak of thermal emission is $\sim 0.14 \text{ eV}$, far below the band gap of Si. If thermal radiation were to contribute to the diode signal, its source is from the same spot as the fluorescence radiation. Its cosine angular distribution is not that different from the isotropic distribution of the fluorescence radiation

**Figure 4**

Differences between the linear fit (predicted) motor positions and the measured values are shown for a horizontal calibration using a wrinkled Ti foil. Positioning errors increase significantly when structure is present in the foil.

for angles of emission intercepted by the diodes and, therefore, would have little effect on calibrations.

Calibrations were internally consistent when measured either in vacuum or in air. The presence of air introduces main-beam air scatter into the measurement and increases fluorescence absorption. It is therefore necessary to perform separate calibrations in air and in vacuum.

An important design consideration is the location of the fluorescing foil with respect to the diode array. Even at $0.5\ \mu\text{m}$ thickness a metal foil is capable of producing measurable powder diffraction intensities. Fig. 5 illustrates a horizontal calibration at 12 keV with the metal foil positioned upstream of the diode array. Oscillations in the difference plot result from a complex mixture of low-order powder rings passing across the individual diodes during calibration. By placing the metal foil downstream of the diodes, only the much weaker powder lines at angles larger than 110° could affect the diode signal.

One important benefit of accurate beam-position measurement, in addition to keeping the beam centered on the slits, is to keep the monochromator crystals exactly parallel for maximum intensity. In fact, using maximization of the intensity as a means of keeping the beam centered on the slits is less accurate than using the beam-position monitor, since peak intensity is relatively insensitive to angular position at low energy. Fig. 6 shows a tuning curve from an Si(111) liquid-nitrogen-cooled monochromator at 8 keV using a Ti foil. In-plane rotation of the second crystal with respect to the first, *i.e.* tune, changes the vertical angle of the output beam resulting in a vertical beam movement at the diode array. If no distortions are present on the first or second crystal, the difference/sum slope is linear with tune. Once the difference/sum value for best tune has been established, deviation from this target can be used, in combination with the difference/sum *versus* tune angle slope, to directly determine the amount and sign of the tune angle correction.

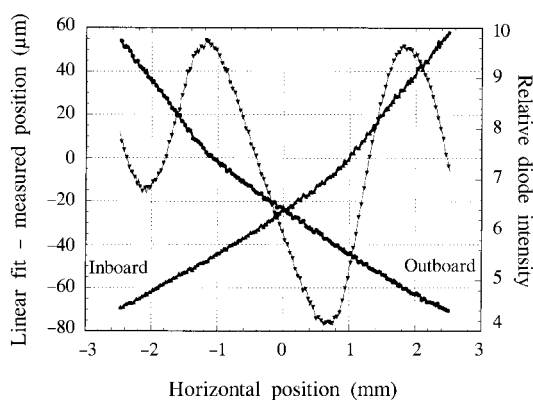


Figure 5

Horizontal calibration at 12 keV in vacuum with Cr metal positioned upstream of the diode array. Oscillations in the difference plot result from a complex mixture of low-order powder rings passing on and off the individual diodes during calibration. By orienting the metal foil downstream of the diodes, interaction with these reflections is avoided.

A straight line has been drawn through the difference/sum curve to estimate linearity over the entire tune curve. As with the vertical calibrations, deviations from linearity appear symmetric about the center of the tune range. The region of most interest is the center (FWHM) of the tune curve. Within the FWHM region the deviation between the data and linear fit is $0.26\ \mu\text{rad}$ r.m.s. This translates into a vertical deviation from linearity of $2.8\ \mu\text{m}$ r.m.s., which is in accordance with the results of the vertical calibrations.

Tuning curves can provide a wealth of information about the status of the monochromator. Deviations from linearity in the difference/sum slope can be used to detect distortions in the first or second crystal. Twisting of the sagittally focusing second crystal results in an expanded rocking-curve width and non-linear vertical movement with tune angle. If the monochromator is water-cooled instead of liquid-nitrogen-cooled, excessive heating can occur in the first crystal. Fig. 7 shows a tuning curve taken at 8 keV using a water-cooled Si(111) crystal at 19ID. The width of the curve is 30% greater than when measured under liquid-nitrogen cooling, indicating significant heating of the first crystal. The abrupt change in slope near the mid-point of the curve is indicative of a thermal bump on the first crystal. Similar changes were observed at 12 keV under water-cooling conditions.

In the same manner the horizontal displacement of the beam is measured as a function of roll angle. Table 2 lists calibration data as a function of tune angle (vertical direction) and roll angle (horizontal direction). Beam deflection is proportional to the roll angle and the sine of the Bragg angle, leading to different calibration values at 8 and 12 keV.

Once the difference/sum *versus* tuning angle calibration has been established for a number of energies, interpolations can be computed to cover intermediate energies. Because the difference/sum calibrations contain magnitude

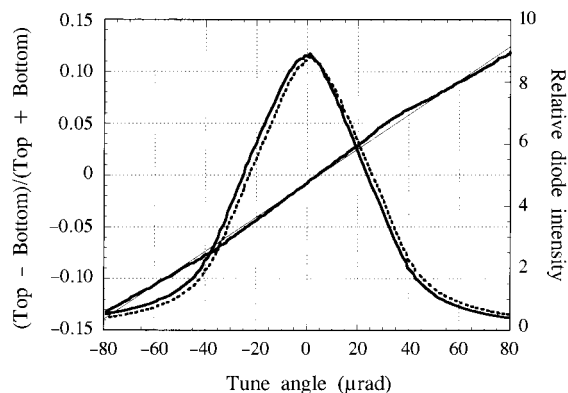


Figure 6

Tuning curve at 8 keV in vacuum from a liquid-nitrogen-cooled Si(111) monochromator as measured by the top (dashed) and bottom (solid) diodes with Ti metal. A line has been drawn through the difference/sum curve to estimate linearity over the full range. A linear fit to the FWHM region produces the tuning calibration, with an estimated error of $0.26\ \mu\text{rad}$ r.m.s., corresponding to a beam position error at the array of $2.8\ \mu\text{m}$ r.m.s.

and direction information, steering of the first or second crystal can be performed rapidly and precisely when an angular correction is needed. Fig. 8 shows beam movement over a 12 h period recorded at ~ 59 m from the source in 3 s intervals using the diode array. For clarity, the horizontal beam position has been offset by $40 \mu\text{m}$. Beam stability is very good, with the average displacement $8 \mu\text{m}$ r.m.s. vertically and $3 \mu\text{m}$ r.m.s. horizontally. Shorter measuring times, *i.e.* < 1 s, show displacement values $\sim 20\%$ greater.

Two trends are evident in Fig. 8: first, a slow drift in beam position, totaling $80 \mu\text{m}$ vertical and $17 \mu\text{m}$ horizontal over 12 h, and second, distinct changes in beam position with a period of 3.7 h. We believe that the former is caused by changes in the storage ring. The latter corresponds to the time interval between fills of the monochromator liquid-nitrogen storage vessel. We know that the temporary pressure rise of 2–3 p.s.i. during refill induces a small amount of angular movement in the first crystal mount, resulting in displacement of the monochromatic beam. In principle, when using only one beam-position monitor, it is not possible to distinguish between beam position and beam angle and, likewise, between beam displacement due to orbit shifts and monochromator-induced movements. We therefore intend to install a similar device in the high-vacuum section immediately downstream of the monochromator. However, at present a single device is successfully used to correct tune losses when changing the energy of the monochromator. This is possible because motions of the white beam, besides momentary fluctuations that are too fast to be compensated, are very slow. In a first approximation the white beam can be considered stable over the time frame that the beam-position information is used to correct loss of tune.

The high position sensitivity of the array suggests that the device can be used for tune stabilization at much higher energies than 12 keV. To operate at energies above 25 keV it may be necessary to increase signal strength. Signal levels could be increased by changing to different metals, such as

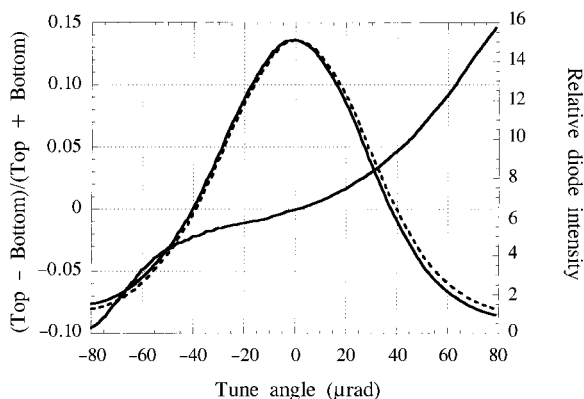


Figure 7

Tuning curve from a water-cooled Si(111) monochromator at 8 keV in vacuum with a Cr foil. The abrupt change in difference/sum slope is indicative of a thermal bump on the first crystal, leading to changes in beam position at the diode array.

Fe ($K_{\text{edge}} 7112$ eV, $K_{\alpha 1} 6404$ eV) or Co ($K_{\text{edge}} 7709$ eV, $K_{\alpha 1} 6930$ eV), which have increased absorption cross sections for high-energy X-rays and still relatively long emission wavelengths. Signal strength may also be enhanced by increasing foil thickness. At 36 keV, for example, a $5 \mu\text{m}$ -thick Fe foil would absorb 2% of the incident beam, with an average of only 12% self-absorption of the fluorescent radiation.

One of the advantages of positioning the diode array upstream of the crystallographic timing shutter is that the beam can be monitored continuously. In macromolecular crystallography, exposing the sample to X-rays can cause sample decay, even when the sample is cooled by a low-temperature nitrogen gas stream. The timing shutter only opens during data collection and is closed when the CCD detector reads out data. Readout time is 1.8 s for full frame images at 19ID. Under software control, data collection time could be used to integrate the signals, while the readout time could be used to correct beam position between exposures if necessary. Data collection time would not be increased and the sample would not incur additional X-ray exposure.

In contrast to similar commercial devices which have narrow fixed openings (typically 2 mm or less), the 8 mm-wide (minimum) opening in the array allows considerable flexibility in monitoring changes in beam position. This makes the device useful for coarse adjustments, as might be encountered when moving beamline components during installation of a mirror. Depending upon the application, this opening could be narrowed to increase diode sensitivity or expanded to widen the displacement coverage.

This device should prove useful on bending-magnet beamlines, even at second-generation synchrotron facilities, since detection efficiency is high for the fluorescing energy and absorption by the thin metal foil is low.

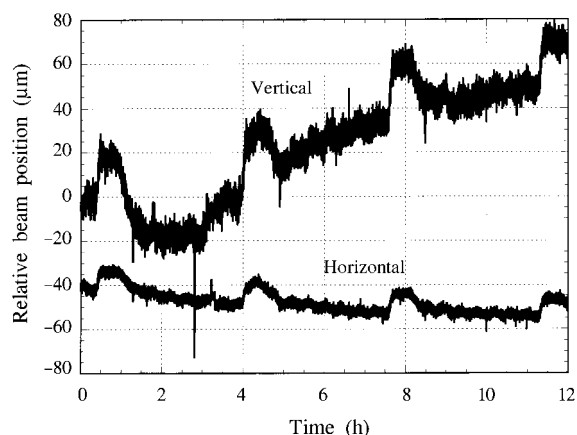


Figure 8

Vertical and horizontal beam movement at 12 keV over time with the beam-position monitor located at ~ 59 m from the source. For clarity, the horizontal beam position has been offset by $40 \mu\text{m}$. Periodic (3.7 h) shifts in beam position result from monochromator movement caused by pressure changes during filling of the monochromator liquid-nitrogen storage vessel. Slow vertical and horizontal drifts are believed to be due to changes in the electron orbit during the measuring period.

4. Summary

A low-cost position-sensitive PIN diode array has been constructed to detect monochromatic beam movement in both the vertical and horizontal direction. Accurate calibrations have been performed, showing the diode array capable of determining changes in beam position at the 1–2 μm level using short-range linear approximations. Because the PIN diodes are positioned away from the direct X-ray beam, diode linearity is maintained at all undulator power levels. After calibration, the device provides magnitude and direction of a change in beam position, making it possible to compute exact position corrections. The device combines high sensitivity with wide spacing between diodes, allowing the array to be used also for coarse adjustments, as might be encountered during beamline reconfigurations. This opening could be altered, according to need, to increase diode sensitivity or expand the operating displacement range. By optimizing characteristics of the metal foil for absorption, thickness and fluorescent radiation, the diode array could be tailored for use at energies exceeding 30–40 keV.

This work was supported by the US Department of Energy, Basic Energy Sciences, Office of Science, under contract number W-31-109-ENG-38.

References

- Alkire, R. W. & Rotella, F. J. (1997). *J. Appl. Cryst.* **30**, 327–332.
- Bergonzo, P., Brambilla, A., Tromson, D., Marshall, R. D., Jany, C., Foulon, F., Gauthier, C., Solé, V. A., Rogalev, A. & Goulon, J. (1999). *J. Synchrotron Rad.* **6**, 1–5.
- Billing, M. (1988). *Nucl. Instrum. Methods Phys. Res. A*, **266**, 144–154.
- Bouldin, C. E., Forman, R. A. & Bell, M. I. (1987). *Rev. Sci. Instrum.* **58**(10), 1891–1894.
- Cauchois, Y. & Senemaud, C. (1978). *Wavelengths of X-ray Emission Lines and Absorption Edges, International Tables of Selected Constants*, Vol. 18, pp. 84–132. New York: Pergamon Press.
- Fauchet, A. M., Biscardi, R., Singh, O., Yu, L. H., Hanna, S., Stefan, P. & NSLS Staff (1992). *Nucl. Instrum. Methods Phys. Res. A*, **319**, 8–17.
- Gauthier, C., Goujon, G., Feite, S., Moguiline, E., Braicovich, L., Brookes, N. B. & Goulon, J. (1995). *Physica B*, **208/209**, 232–234.
- Hahn, U., Brefeld, W., Hesse, M., Schneider, J. R., Schulte-Schrepping, H., Seebach, M. & Werner, M. (1998). *J. Synchrotron Rad.* **5**, 627–629.
- Henke, B. L., Gullikson, E. M. & Davis, J. C. (1993). *Atom. Data Nucl. Data Tables*, **54**(2), 234–239.
- Jemian, P. R. & Long, G. G. (1990). *J. Appl. Cryst.* **23**, 430–432.
- Johnson, E. D. & Overslizen, T. (1989). *Rev. Sci. Instrum.* **60**(7), 1947–1950.
- Khalid, S., Chance, B. & Zhang, M. (1990). *Nucl. Instrum. Methods Phys. Res. A*, **291**, 431–434.
- Koyama, A., Sasaki, S. & Ishikawa, T. (1989). *Rev. Sci. Instrum.* **60**(7), 1953–1956.
- Miyahara, T. & Mitsuhashi, T. (1992). *Rev. Sci. Instrum.* **63**(1), 538–540.
- Mortazavi, P., Woodle, M., Rarback, H., Shu, D. & Howells, M. (1986). *Nucl. Instrum. Methods Phys. Res. A*, **246**, 389–393.
- Sakae, H., Aoyagi, H., Oura, M., Kimura, H., Ohata, T., Shiwaku, H., Yamamoto, S., Sugiyama, H., Tanabe, K., Kobashi, K. & Kitamura, H. (1997). *J. Synchrotron Rad.* **4**, 204–209.
- Schildkamp, W. & Pradervand, C. (1995). *Rev. Sci. Instrum.* **66**(2), 1956–1959.
- Shu, D., Ding, H., Barraza, J., Kuzay, T. M., Haeffner, D. & Ramanathan, M. (1998). *J. Synchrotron Rad.* **5**, 632–635.
- Silfhout, R. G. van (1999). *J. Synchrotron Rad.* **6**, 1071–1075.
- Southworth, S. H. & Cowan, P. L. (1992). *Nucl. Instrum. Methods Phys. Res. A*, **319**, 51–55.
- Storb, Ch., Dedek, U., Weber, W., Lengeler, B. & Schuster, M. (1991). *Nucl. Instrum. Methods Phys. Res. A*, **306**, 544–548.
- Vaughn, D. (1986). Editor. *Center for X-ray Optics X-ray Data Booklet*, §2, pp. 19–20. Lawrence Berkeley Laboratory, University of California, Berkeley, CA 94720, USA.
- Warwick, T., Shu, D., Rodricks, B. & Johnson, E. D. (1992). *Rev. Sci. Instrum.* **63**(1), 550–553.